doi.org/10.36721/PJPS.2026.39.6.159.1

Andrographolide mitigates paraquat-induced pulmonary injury via PI3K/Akt/PPARγ pathway-mediated regulation of EMT and oxidative stress

Degang Zhang[1,2,3]*, Shengming Zhao[2,3], Jiayi Xiao[2,3], Qinyi Cai[2,3] and Bo Zhao[2,3]
[1]Department of Respiratory and Critical Care Medicine, Lanzhou University Second Hospital, Lanzhou, China
[2]The Second Clinical Medical School, Lanzhou University, Lanzhou, China
[3]Lanzhou University, Lanzhou, China

Abstract: **Background**: Paraquat (PQ) poisoning causes acute pulmonary injury via oxidative stress and epithelial-mesenchymal transition (EMT), with limited treatment options. **Objectives**: This study investigated whether andrographolide (Andro) alleviates PQ-induced lung damage and the underlying mechanisms. **Methods**: PQ-induced pulmonary injury was established in C57BL/6J mice. Animals were assigned to Control, Andro, PQ and PQ +Andro groups. Lung pathology, oxidative stress markers (MPO, ROS, MDA, SOD, CAT), EMT markers (E-cadherin, α-SMA), and PI3K/Akt/PPARγ pathway proteins were assessed *in vivo* and in MLE-12 cells, with PI3K inhibition using LY294002. **Results**: Andro significantly improved survival, reduced alveolar injury and collagen deposition, and suppressed oxidative stress by downregulating ROS/MDA/MPO and enhancing SOD/CAT. It suppressed EMT by upregulating E-cadherin and reducing α-SMA. Andro inhibited PI3K/Akt activation and increased PPARγ expression. LY294002 partially reproduced these effects, supporting pathway involvement. **Conclusion**: Andro mitigates PQ-induced lung damage by limiting oxidative stress and EMT via the PI3K/Akt/PPARγ pathway. These findings provide preclinical evidence for its further investigation as a candidate protective agent.

Keywords: Andrographolide; Epithelial-mesenchymal transition; Lung injury; Oxidative stress; Phosphatidylinositol-3-kinase

Submitted on 13-09-2025 – Revised on 30-10-2025 – Accepted on 07-11-2025

INTRODUCTION

Paraquat (PQ), a non-selective herbicide, is extensively used in agriculture for its rapid action and low cost (Somu *et al.*, 2020). However, PQ exerts severe toxic effects on humans, causing multi-organ injuries, particularly in the lungs, liver, kidneys, and heart (Qin *et al.*, 2024). The lung is the primary target because PQ structurally resembles polyamines, allowing its uptake and accumulation in alveolar epithelial cells, which leads to oxidative damage and progressive respiratory failure (Somu *et al.*, 2020). Severe lung injury following PQ exposure often results in acute respiratory distress and a high risk of mortality. Despite advances in supportive care, no effective antidotes exist, and the mortality rate remains high (Buckley *et al.*, 2021; Lekei *et al.*, 2020; Lihua *et al.*, 2023). Therefore, elucidating the mechanisms of PQ-induced lung injury and exploring potential therapeutic strategies remain urgent priorities.

Emerging evidence indicates that epithelial-mesenchymal transition (EMT) plays a critical role in PQ-induced pulmonary toxicity (Xia *et al.*, 2022; Yi *et al.*, 2021). EMT is characterized by loss of epithelial polarity and acquisition of mesenchymal phenotypes, with alveolar epithelial cells differentiating into myofibroblasts and fibroblasts, the principal contributors to pulmonary fibrosis (Andugulapati *et al.*, 2020; Lee *et al.*, 2021). During the initial stage of acute lung injury, EMT-mediated generation of these mesenchymal cells aids in repairing damaged epithelium (Marconi *et al.*, 2021). However, excessive collagen deposition by these cells eventually leads to irreversible pulmonary fibrosis (Spagnolo *et al.*, 2021). In parallel, oxidative stress is considered to be another key mechanism in PQ-induced pulmonary toxicity, as PQ promotes excessive production of reactive oxygen species (ROS), causing cellular damage and necrosis (Memarzia *et al.*, 2024). Consequently, strategies that target both oxidative stress and EMT are considered promising for mitigating PQ-induced pulmonary injury.

Andrographolide (Andro), the major bioactive diterpene lactone isolated from *Andrographis paniculata*, is recognized for its anti-inflammatory, antiviral, and antioxidant properties (Burgos *et al.*, 2020; Kumar *et al.*, 2020). Previous studies have shown that Andro can protect alveolar epithelial cells by reducing oxidative stress and inhibiting EMT (Karkale *et al.*, 2018; Li *et al.*, 2020), primarily through suppression of ROS generation and modulation of antioxidant enzymes such as superoxide dismutase (SOD) and malondialdehyde (MDA) (Kanazawa *et al.*, 2021; Mussard *et al.*, 2020). However, whether Andro can specifically protect against PQ-induced pulmonary toxicity and the underlying molecular mechanisms remains unclear. Considering the unique

**Corresponding author:* e-mail: zhangdg18@lzu.edu.cn

pathophysiology of PQ poisoning, marked by excessive oxidative stress and EMT-driven fibrosis, it is critical to investigate the protective potential of Andro and delineate the signaling pathways involved.

Therefore, in this study, we established a mouse model of PQ-induced pulmonary injury to investigate whether Andro mitigates PQ-induced lung toxicity by regulating the EMT process and oxidative stress. Our results demonstrate that Andro alleviates oxidative damage and suppresses EMT, at least in part through regulation of the PI3K/Akt/PPARγ signaling pathway, thereby providing a mechanistic link between its pharmacological effects and the key pathogenic processes underlying PQ-induced lung injury.

MATERIALS AND METHODS

Establishment of a laboratory animal model

Female C57BL/6J mice (4-6 weeks old, 20 ± 2 g) were purchased from the Lanzhou Institute of Veterinary Medicine, Chinese Academy of Agricultural Sciences. Animals were housed under standard laboratory conditions with free access to standard chow and drinking water.

The animals were randomly assigned to either a control group (no PQ) or a model group (PQ-induced lung injury). Acute lung injury was induced via intraperitoneal injection of PQ at 20 mg/kg, a dose validated in previous studies to reliably induce pulmonary damage (Zhang *et al.*, 2023). Lung tissues were collected 72 hrs post-PQ administration.

To evaluate the effects of Andro, mice were subsequently allocated into four groups (n = 10 per group), as follows: Control group: received sterile saline intragastrically as a vehicle control. Andro group: administered Andro at 50 mg/kg/d intragastrically for three consecutive days without PQ exposure, serving as a drug safety control. PQ group: received 20 mg/kg of PQ intraperitoneally with no subsequent treatment. PQ+ Andro group: received 20 mg/kg of PQ intraperitoneally, followed 1 h later by Andro (50 mg/kg/day) intragastrically for three consecutive days.

The dosing regimen and timing of Andro administration were based on preliminary experiments demonstrating its protective efficacy against lung injury (Zhang *et al.*, 2023). At 72 hr after PQ administration, all mice were euthanized under isoflurane anesthesia, and lung tissues were harvested for subsequent analyses.

Lung histopathology analysis

After tissue collection, lung samples were gently rinsed with phosphate-buffered saline (PBS) to remove residual blood and fixed in 4% paraformaldehyde (Cat: BL539A) (Biosharp, Hefei, China) for 48 hrs. Fixed tissues were dehydrated through a graded ethanol series, cleared in xylene, and embedded in paraffin. Paraffin blocks were sectioned into 5 μm slices, mounted on glass slides, and baked at 80°C overnight for complete adhesion. Sections were deparaffinized with xylene and rehydrated through a descending ethanol series, followed by three PBS (Gibco, Carlsbad, CA, USA) washes. Hematoxylin-eosin (HE) and Masson's trichrome staining were performed using commercial kits (Solarbio, Beijing, China) according to the manufacturer's instructions. Stained slides were sealed with neutral gum mounting medium and examined under an inverted microscope (Olympus CKX53, Tokyo, Japan).

For histopathological evaluation, all lung tissue samples were randomly coded by independent personnel to conceal group allocation. The investigators who performed microscopic observation and scoring were blinded to the experimental groups. Histological assessment was independently conducted by two experienced pathologists who were unaware of the study design or treatment assignments.

Histopathological evaluation was based on characteristic lung injury features, including alveolar congestion, hemorrhages, alveolar wall thickening, structural destruction, and hyaline membrane formation. The severity of lung injury was scored semi-quantitatively on a 5-point scale (from 0 to 4), with 0 indicating no lesions and 4 representing the most severe damage (Yoshida *et al.*, 2012).

Immunohistochemistry (IHC) analysis

Paraffin-embedded lung sections were dried, deparaffinized in xylene, and rehydrated through a graded ethanol series. Immunohistochemical staining was conducted using commercial kits (Zsbio, Beijing, China) following the manufacturer's instructions. Antigen retrieval and endogenous peroxidase blocking were carried out according to standard procedures. Subsequently, sections were incubated overnight at 4°C with the following primary antibodies: anti-E-cadherin (1: 2000, Proteintech, 20874-1-AP) and anti-α-smooth muscle actin (α-SMA, 1: 1500, Proteintech, 14395-1-AP). After washing with PBS, slides were incubated with the secondary antibody (1:1000, BioSharp, BL1600A) for 1 h at room temperature, followed by incubation with the Streptavidin-Biotin Complex (SABC) reagent at 37°C for 20 mins. After three PBS washes (10 mins each), sections were incubated with DAB substrate for 8 mins. The stained sections were ultimately visualized and imaged under a microscope (Olympus CKX53, Tokyo, Japan) for histological analysis.

Cell culture

Murine lung epithelial cells (MLE-12) were supplied from ATCC for *in vitro* experiments. Cells were maintained in a 1:1 ratio of DMEM and F-12 nutrient medium (Gibco, Carlsbad, USA) supplemented with 10% certified fetal bovine serum (Biological Products Trading Co., Ltd., Changsha, China) and 1% penicillin/streptomycin antibiotics (Biosharp, Hefei, China). Cells were incubated at 37°C in a humidified atmosphere containing 5% CO_2.

Experimental grouping in-vitro

MLE-12 cells were seeded in 96-well plates at a density of 1×10^4 cells per well and cultured for 24 hrs. For treatment, the cells were then divided into six groups: (1) Control, (2) Andrographolide (Andro, 25 μM) alone, (3) LY294002 (10 μM) alone, (4) Paraquat (PQ, 950.2 μM) alone, (5) Andro + PQ, and (6) LY294002 + Andro + PQ. For the corresponding groups, cells were pretreated with Andro (25 μM) or LY294002 (10 μM) for 6 hrs. Subsequently, except for the Control andro alone and LY294002 alone groups, all other groups were exposed to PQ (950.2 μM) for an additional 24 hrs to induce cellular injury. The PQ concentration (950.2 μM) was selected based on previous reports demonstrating that this dose reliably induces oxidative stress and epithelial injury in MLE-12 cells while maintaining acceptable cell viability for mechanistic evaluation (Zhang *et al.*, 2023). Preliminary experiments in our laboratory further confirmed that this concentration produced reproducible cytotoxicity suitable for pharmacological intervention assays.

Cell viability assay

Cell viability was assessed using the CCK-8 Kit (Beyotime, Shanghai, China) in accordance with the manufacturer's protocol. After the indicated treatments, 10 μl of CCK-8 solution was added to each well, followed by incubation at 37°C in a humidified incubator (Thermo Scientific™ Forma™ 310, USA) containing 5% CO_2 for 1 h. Cell growth was then observed with an inverted microscope (Olympus CKX53, Tokyo, Japan). The optical density (OD) was measured at 450 nm using a microplate reader (Multiskan FC, ThermoFisher, USA). All measurements were performed in triplicate and normalized to the control group.

ROS detection

Reactive oxygen species (ROS) levels were determined both *in-vivo* (bronchoalveolar lavage fluid, BALF) and *in vitro* (MLE-12 cells) using the DCFH-DA fluorescent probe (Biosharp, Hefei, China), following the manufacturer's protocol. For *in-vivo* analysis, BALF samples were collected from mice and incubated with 5 μM DCFH-DA at 37°C for 30 mins in the dark to allow probe uptake. After incubation, fluorescence intensity corresponding to intracellular ROS was quantified using flow cytometry (CytoFLEX, Beckman Coulter, USA). For *in vitro* experiments, MLE-12 cells (1×10^6 per well) were seeded in 6-well plates and cultured for 24 hrs. After the indicated treatments, cells were washed twice with PBS and incubated with 5 μM DCFH-DA for 30 mins at 37°C in a humidified CO_2 incubator. Fluorescent images were acquired using an Olympus fluorescent microscope (IX 53, Tokyo, Japan). All experiments were performed in triplicate, and fluorescence signals were normalized to the untreated control group to ensure comparability. Negative controls without DCFH-DA staining were included to exclude background fluorescence.

Measurement of oxidative stress markers (SOD, CAT, and MDA)

Lung tissues were mechanically homogenized on ice and lysed in RIPA lysis buffer (Beyotime, Shanghai, China) to extract total proteins. The supernatants were collected after centrifugation at 12,000 rpm for 10 mins at 4°C (Eppendorf 5417R, Germany). The levels of SOD, CAT, and MDA were measured using commercial kits (Njjcbio, Nanjing, China) as recommended by the manufacturer. For *in-vitro* analysis, MLE-12 cells were harvested and centrifuged (1000 rpm, 10 mins) at 4°C. The cell pellets were resuspended in lysis buffer and disrupted using an ultrasonic cell splinter (JXFSTPRP-II, Ningbo, China) at a power of 300W with 5s sonication pulses and 30s intervals for five cycles to ensure complete lysis. The lysates were centrifuged, and the resulting supernatants were analyzed for SOD, MDA, and CAT levels using the same commercial kits. Absorbance values were measured at the corresponding wavelengths with a microplate reader (Mulltiskan FC, ThermoFisher, USA), and results were normalized to total protein concentration. All assays were performed in triplicate to ensure reproducibility.

Western blotting

Total proteins were extracted from MLE-12 cells or lung tissues using RIPA lysis buffer (Beyotime, Shanghai, China). Protein concentrations were determined using the BCA assay to ensure equal loading. Equal amounts of protein samples were separated on 10% SDS-PAGE gels under the following conditions: 80 V for 20 mins (stacking gel) and then 120 V for 80 mins (separating gel). Following electrophoresis, protein bands were transferred onto a PVDF membrane using a wet transfer system at 400 mA for 60 min. After washing with TBST buffer, membranes were blocked with 5% bovine serum albumin (BSA) for 1 h at room temperature. Then, the membranes were incubated overnight at 4°C with the following validated primary antibodies. Antibodies sourced from Cell Signaling Technology (Danvers, MA, USA) included MPO (Rabbit pAb, 1:1,000; Cat: 15178T); p-PI3K (Rabbit pAb, 1:1,000; Cat: 4228T); PI3K (Rabbit pAb, 1:1,000; Cat: 4292S); p-Akt (Rabbit pAb, 1:1,000; Cat: 4060T); and Akt (Rabbit pAb, 1:1,000; Cat: 9272S). Antibodies from Proteintech (Wuhan, China) included PPARγ (Rabbit pAb, 1:20,000; Cat: 66936-1-Ig), E-cadherin (Rabbit pAb, 1:5,000; Cat: 20874-1-AP), and α-SMA (Rabbit pAb, 1:5,000; Cat: 14395-1-AP). The specificity for these antibodies has been previously validated by the manufacturer using genetic approaches in relevant human cell lines. The antibody against the loading control, β-actin (1:2,500; Cat: BL071A), was from BioSharp (Hefei, China).

After three washes with TBST (10 mins per wash), membranes were incubated with HRP-labeled IgG (IgG-HRP, 1:10,000; Cat: BL1600A) (BioSharp, Hefei, China) for 60 min at room temperature. Protein bands were

visualized using a high-sensitivity ECL kit (Biosharp, Hefei, China) in accordance with the manufacturer's protocols, and densitometric analysis was conducted using ImageJ software.

Statistical analysis

All data are expressed as the mean ± standard deviation (SD). Statistical analyses were performed using GraphPad Prism 8.0 (San Diego, USA). A one-way ANOVA followed by Dunnett's multiple comparison tests was performed to evaluate differences among groups. Statistical significance was defined as a P-value < 0.05 and $P < 0.01$, indicating high significance.

RESULTS

Andro attenuates PQ-induced pulmonary damage by reducing inflammatory responses, oxidative stress, and EMT in mice

A mouse model of PQ-induced lung injury was established to examine the protective effect of Andro (Fig. 1A). PQ exposure drastically decreased survival to 30% at 48 hrs, whereas Andro intervention significantly improved survival to 70% ($P < 0.01$), indicating a protective role in acute PQ toxicity (Fig. 1B).

Histopathological analysis revealed that PQ induced severe alveolar disruption, congestion, hemorrhage, and lumen collapse, reflected by significantly elevated lung injury scores. Andro treatment preserved alveolar structure and significantly reduced lung injury scores ($P < 0.01$ vs. PQ) (Figs. 1C-E). Masson staining further demonstrated excessive collagen deposition in PQ-exposed lungs, which was attenuated by Andro ($P < 0.01$), supporting its anti-fibrotic efficacy (Figs. 1D, 1F).

MPO, a specific indicator of the inflammatory response, was significantly elevated following PQ exposure ($P < 0.01$). Andro treatment reduced MPO levels ($P < 0.01$ vs. PQ group), indicating its anti-inflammatory effect. (Figs. 1G, 1H)

To determine oxidative stress, ROS, MDA, SOD, and CAT levels were assessed. PQ significantly elevated ROS and MDA levels (Figs. 2A-C) but decreased SOD and CAT levels ($P < 0.01$ for all) (Figs. 2D, 2E), indicating severe oxidative damage. Andro reversed these changes by reducing ROS and MDA and restoring CAT and SOD levels ($P < 0.01$ for all), confirming its antioxidant capacity.

EMT was assessed through the expression levels of E-cadherin and α-SMA. E-cadherin is a key marker of lung epithelial cells, primarily localized to the cell membrane of epithelial cells of the alveoli and bronchi (Braga 2016). In contrast, α-SMA is abundantly expressed in smooth muscle cells surrounding airways, bronchi, and blood vessels and in myofibroblasts that proliferate during pulmonary fibrosis. As a hallmark of mesenchymal cells, α-SMA serves as a core indicator of the EMT process (Darby *et al.*, 2016). PQ exposure significantly downregulated E-cadherin ($P < 0.01$) and upregulated α-SMA ($P < 0.01$), reflecting loss of epithelial phenotype and mesenchymal activation (Figs. 2F, 2G, 2I). Andro treatment restored E-cadherin and suppressed α-SMA levels ($P < 0.01$), indicating suppression of the EMT process (Figs. 2F-I).

Taken together, these results demonstrate that Andro significantly improves survival and attenuates PQ-induced pulmonary injury by reducing inflammatory responses, oxidative damage, and EMT progression, thereby preserving lung structure and function.

Andro suppresses PQ-induced activation of the PI3K/Akt/PPARγ pathway in lung tissues

To investigate the mechanism of Andro-mediated lung protection, Western blotting was employed to assess the PI3K/Akt/PPARγ pathway. PQ exposure markedly increased the p-PI3K/PI3K and p-Akt/Akt ratios while reducing PPARγ expression ($P < 0.01$ for both), indicating PI3K/Akt pathway activation and PPARγ suppression. Nevertheless, Andro treatment significantly attenuated PI3K and Akt phosphorylation levels ($P < 0.01$) and restored PPARγ expression ($P < 0.01$) (Figs. 3A-D). These results indicate that Andro mitigates PQ-induced lung damage, at least partly, by blocking the PI3K/Akt pathway and upregulating PPARγ, thereby modulating downstream processes such as EMT and oxidative stress.

Andro alleviates PQ-induced cytotoxicity via the PI3K/Akt/PPARγ signaling pathway in MLE-12 cells

To explore cellular mechanisms of Andro, cell viability was tested by CCK-8 assays, PQ, and the PI3K inhibitor LY294002 on MLE-12 cell viability. PQ (950.2 μM, 24 hrs) significantly reduced cell viability to approximately 50%, while Andro (25 μM) pretreatment significantly improved cell survival ($P < 0.01$). Co-treatment with LY294002 further enhanced the protective effect of Andro ($P < 0.05$) (Figs. 4A–B), suggesting a PI3K-dependent mechanism.

Western blotting analysis showed PQ exposure notably elevated the p-PI3K/PI3K and p-Akt/Akt ratios while suppressing PPARγ expression ($P < 0.05$ for all). Andro reversed these effects, significantly downregulated p-PI3K and p-Akt levels, and restored PPARγ expression ($P < 0.05$) (Figs. 4C-D).

Furthermore, LY294002 further enhanced these effects when combined with Andro, further reduced p-PI3K and p-Akt ($P < 0.01$), and elevated PPARγ expression ($P < 0.05$) (Figs. 4C-D). Thus, these results confirm that Andro exerts its cytoprotective effects by blocking PI3K/Akt activation and restoring PPARγ levels to attenuate the PQ-induced cellular toxicity.

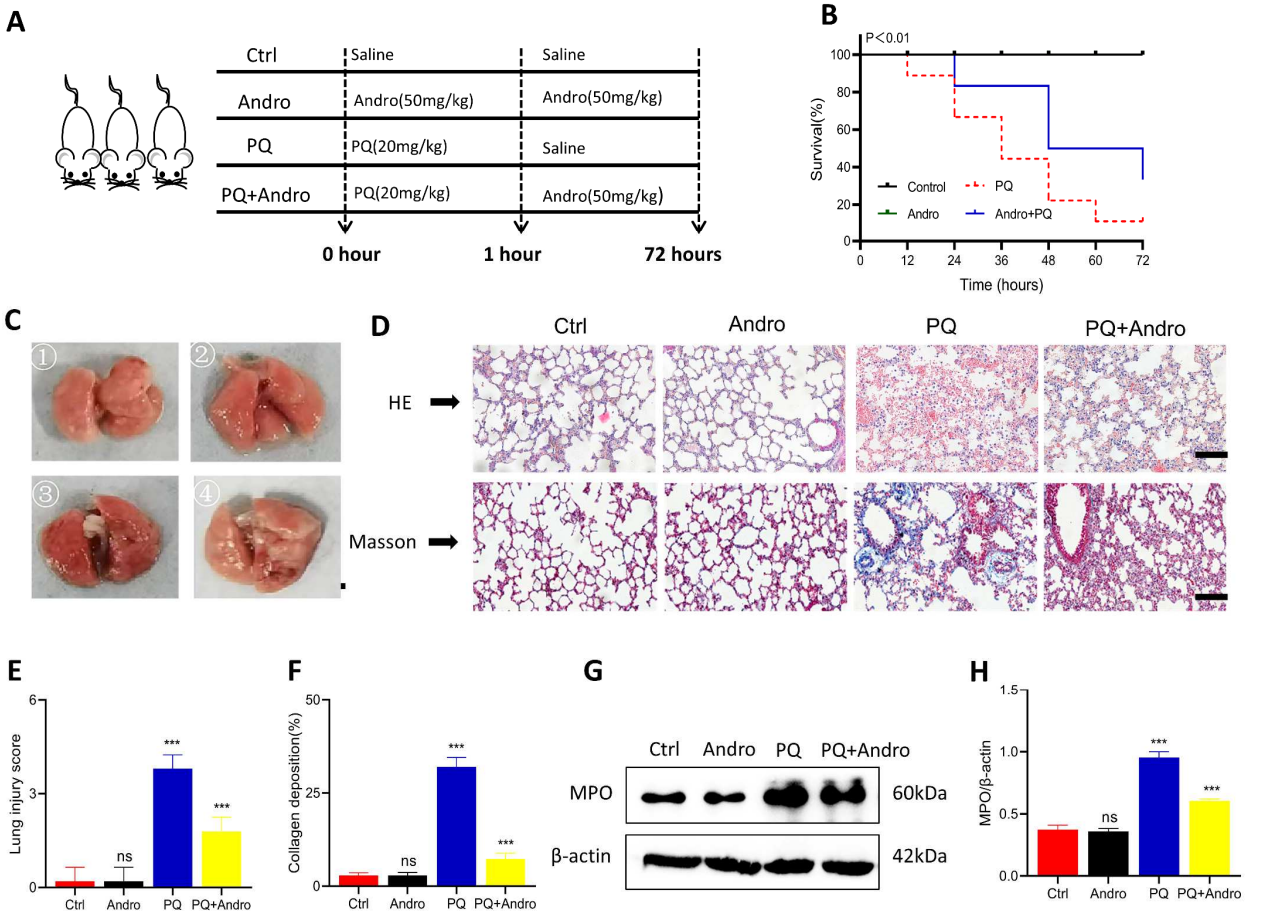

Fig. 1: Andro improves survival and attenuates lung injury in PQ-exposed mice. (A) Experimental design schematic. (B) Andro improved survival rates in PQ-treated mice (n = 10 per group). (C-D) Representative lung morphology and histopathology (H&E and Masson staining, scale bar = 50 μm). (E-F) Quantification of lung injury scores and collagen deposition area. (G-H) MPO level in lung tissues measured by Western blot and densitometry. The statistics are presented as mean ± SD (N = 3). "ns" means no significant difference, $^{**}P < 0.01$.

Andro suppresses PQ-induced oxidative injury and EMT through regulating the PI3K/Akt/PPARγ pathway in cells

To elucidate whether Andro's protective effects involve oxidative stress and EMT regulation, intracellular MDA, ROS, SOD, and CAT levels were measured. Compared with the Control group, PQ exposure markedly increased intracellular MDA and ROS levels, while decreasing the activities of antioxidant enzymes SOD and CAT ($P < 0.01$ for all). Andro pretreatment significantly mitigated oxidative injury, as evidenced by decreased MDA ($P < 0.01$) and ROS levels and elevated SOD ($P < 0.01$) and CAT ($P < 0.05$) activity (Figs. 5A-D). Co-treatment with LY294002 further enhanced the antioxidant effects of Andro, resulting in a more pronounced reduction in ROS and MDA levels ($P < 0.01$ for both), together with a further elevation of antioxidant enzyme activities, including SOD and CAT ($P < 0.01$ and $P < 0.05$, respectively) (Figs. 5A-D). These results indicate that Andro mitigates PQ-induced oxidative stress through suppression of the PI3K/Akt pathway and restoration of PPARγ signaling.

To assess EMT, E-cadherin and α-SMA expressions were examined. Compared with the Control group, PQ exposure significantly upregulated α-SMA and downregulated E-cadherin ($P < 0.01$ for all) (Figs. 5E-G), indicating EMT activation. Andro pretreatment markedly reversed these changes ($P < 0.01$ for all) (Figs. 5E-G), suggesting suppression of EMT. LY294002 further enhanced this effect, reduced α-SMA expression ($P < 0.01$), and elevated E-cadherin expression ($P < 0.05$) (Figs. 5E-G). The Control and Andro-alone groups showed no significant alterations, indicating Andro had no effect on basal EMT markers. These findings demonstrate that Andro effectively inhibits PQ-induced EMT, potentially through regulation of the PI3K/Akt/PPARγ pathway, thereby contributing to its cytoprotective effects against PQ-induced cellular injury.

DISCUSSION

In our study, we demonstrated that Andro significantly attenuates PQ-induced pulmonary injury by suppressing

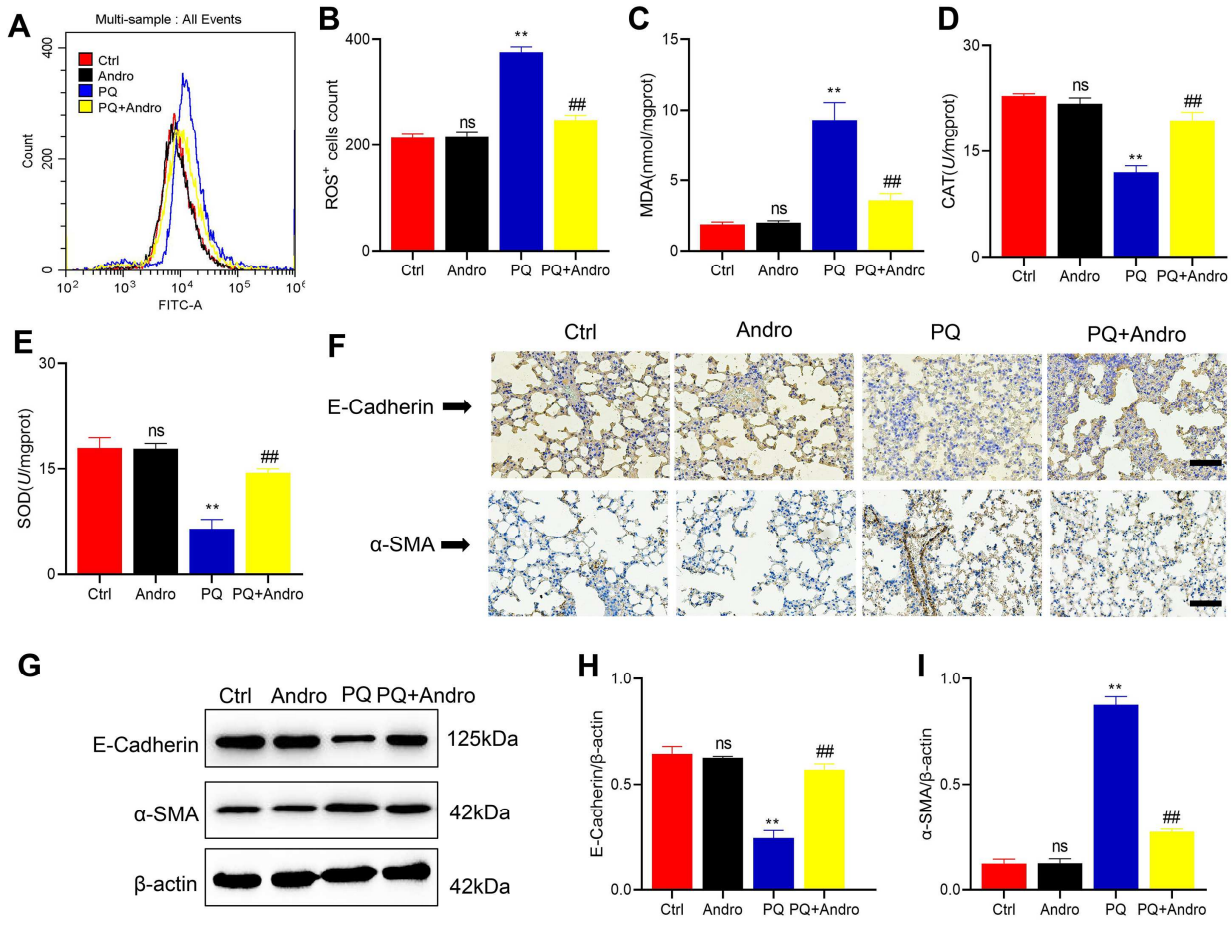

Fig. 2: Andro attenuates PQ-induced oxidative stress and EMT in mice. (A-B) ROS level in BALF and quantification of ROS-positive cells. (C-E) MDA, CAT, and SOD levels in lung tissue. (F) Representative IHC staining of E-cadherin and α-SMA (scale bar = 50 μm). (G-I) Western blot and densitometric analysis of E-cadherin and α-SMA. The statistics are presented as mean ± SD (N = 3). "ns" means no significant difference, $^{**}P < 0.01$.

oxidative stress and EMT. Although previous studies have reported the antioxidant and anti-EMT activities of Andro in other pathological contexts, our work extends these findings by identifying a specific toxicological model and revealing an integrated signaling mechanism. We confirmed that Andro exerts its dual protective actions primarily through modulation of the PI3K/Akt/PPARγ pathway, as further supported by inhibitor experiments using LY294002. Through both *in-vivo* and *in-vitro* experiments, our results revealed a regulatory link between oxidative stress and EMT, positioning PI3K/Akt/PPARγ as a pivotal mediator of Andro's therapeutic action.

PQ-induced lung damage involves oxidative stress and EMT, yet the precise molecular mechanisms and therapeutic potential of Andro in this context remain unclear. Consistent with previous reports, PQ exposure induced typical pathological alterations in lung tissue, including alveolar structural destruction, hemorrhage, and collapse (Tyagi *et al.*, 2019). Remarkably, Andro administration effectively ameliorated these pathological injuries, supporting its protective efficacy and providing a foundation for further mechanistic investigations. The novelty of this study lies in identifying PI3K/Akt/PPARγ as the signaling axis through which Andro modulates both oxidative stress and EMT during PQ-induced lung injury. Accumulating evidence highlights EMT as a critical event in PQ-related pulmonary injury (Gao, *et al.*, 2020; Jia, *et al.*, 2021). In this study, the findings illustrated that Andro markedly reverses PQ-induced EMT by restoring E-cadherin expression and inhibiting α-SMA upregulation both *in-vivo* and *in-vitro*. Furthermore, oxidative stress, driven by excessive ROS generation and mitochondrial redox imbalance, plays a central role in PQ-induced pulmonary damage by promoting lipid peroxidation and depleting antioxidant defenses such as SOD and CAT (Amin, *et al.*, 2021; Memarzia, *et al.*, 2023). Interestingly, our findings also confirmed that Andro alleviates PQ-induced oxidative stress by decreasing ROS and MDA levels while elevating SOD and CAT activity. Emerging evidence has implicated that the PI3K/Akt/PPARγ pathway is a crucial regulator in PQ-induced lung injury (Abu-Eid

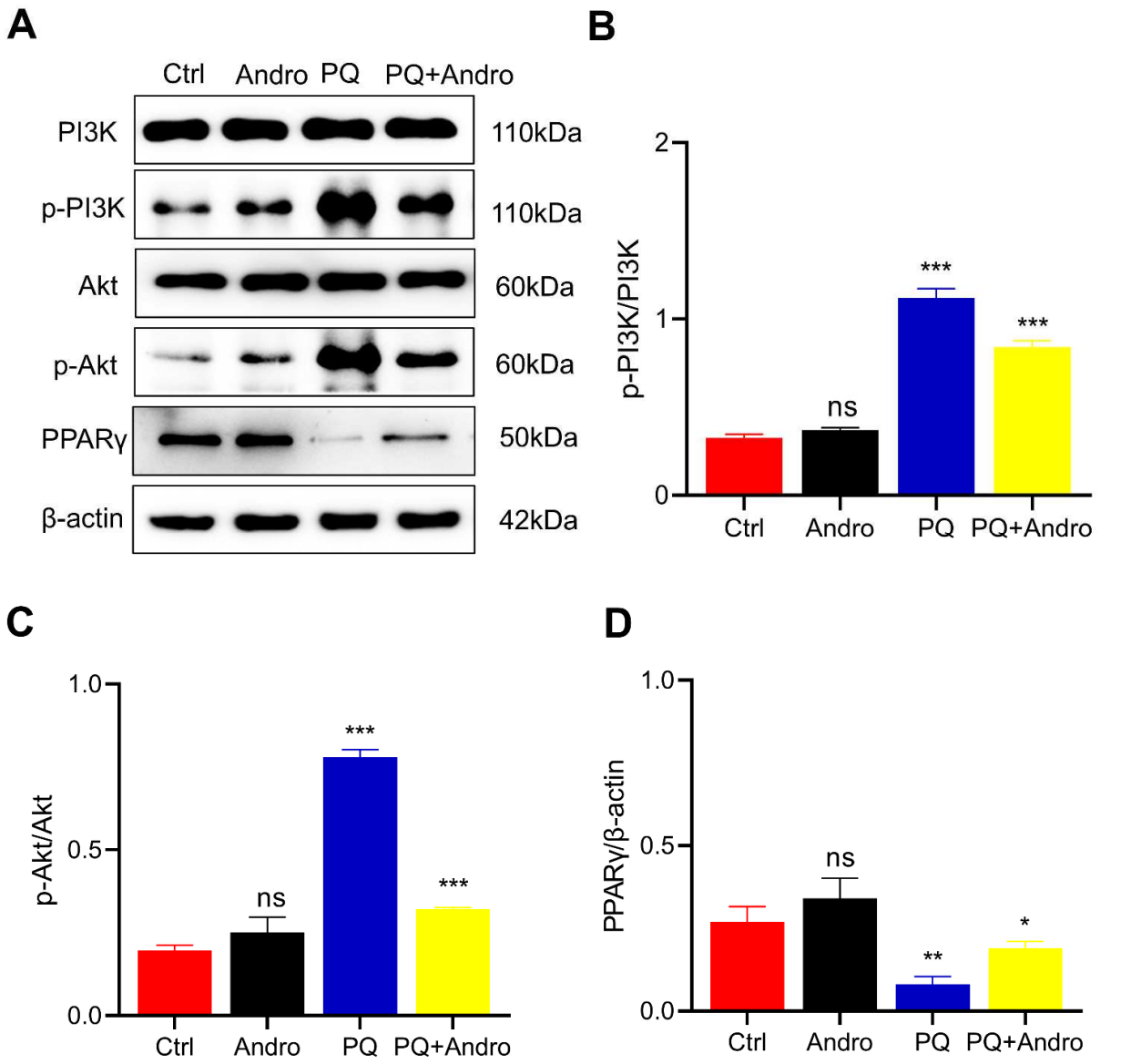

Fig. 3: Andro inhibits the activation of the PI3K/Akt/PPARγ pathway in PQ-induced lung injury in mice. (A) Western blot analysis of PI3K, p-PI3K, Akt, p-Akt, and PPARγ in the lung tissues was measured by western blotting. (B-D) Quantitative analysis of p-PI3K/PI3K, p-Akt/Akt, and PPARγ expression. The statistics are presented as mean ± SD (N = 3). "ns" means no significant difference, $^{**}P < 0.01$.

and Ward, 2021; Glaviano *et al.*, 2023; Meng *et al.*, 2021). Our research provides experimental evidence that Andro confers its lung-protective effects by downregulating the PI3K/Akt/PPARγ pathway. Notably, we identified a novel mechanistic link between the PI3K/Akt/PPARγ pathway and the regulation of both EMT and oxidative stress in PQ-associated lung damage (Chen et al., 2020; Wu et al., 2021). Specifically, we demonstrated that Andro suppressed PI3K/Akt activation and elevated PPARγ expression, leading to decreased ROS and MDA levels, restored antioxidant enzymes (SOD, CAT), and reversal of EMT markers (decreased α-SMA, increased E-cadherin). Importantly, our findings reveal that the PI3K/Akt/PPARγ pathway serves as a central hub coordinating both EMT and oxidative stress in PQ-induced lung toxicity, and Andro's therapeutic efficacy is achieved through its targeted inhibition of this pathway.

This study establishes that Andro's protective activity against PQ-induced lung damage is mediated by its dual regulation of EMT and oxidative stress through the PI3K/Akt/PPARγ pathway, offering a novel therapeutic strategy for PQ-related pulmonary injury. However, several limitations of this study should be acknowledged. First, only a single dose of Andro and a single observation time point were employed, without further optimization of concentration or extension of follow-up duration.

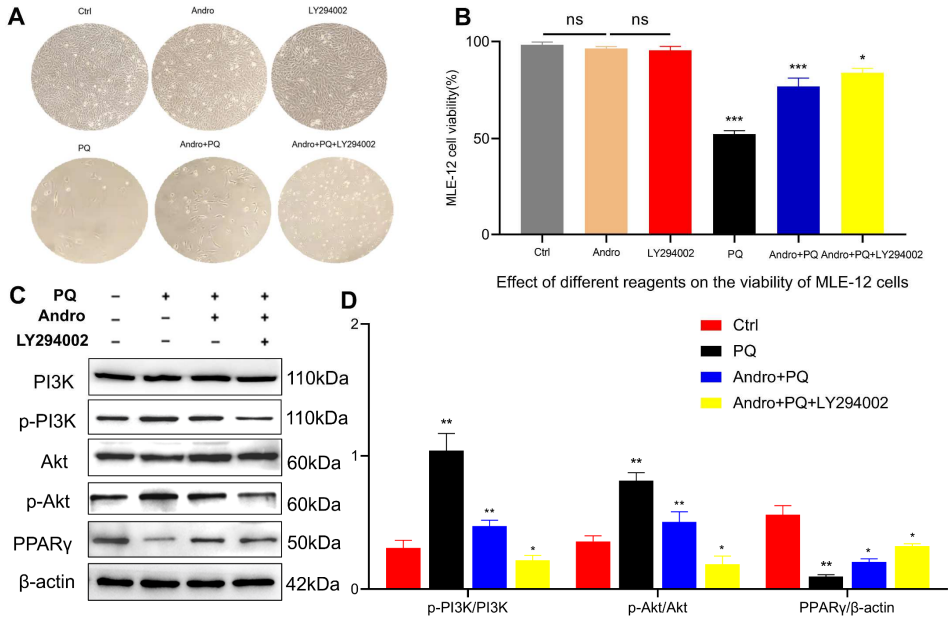

Fig. 4: Andro improves cell viability in PQ-exposed MLE-12 cells via PI3K/Akt/PPARγ pathway inhibition. (A) Representative morphology of MLE-12 cells (10×). (B) Cell viability assessed by CCK-8 assay. (C) Western blot analysis of PI3K, p-PI3K, Akt, p-Akt, and PPARγ. (D) Quantitation of p-PI3K/PI3K, p-Akt/Akt and PPARγ expression. The statistics are presented as mean ± SD (N = 3). "ns" means no significant difference, $^{*}P < 0.05$, $^{**}P < 0.01$.

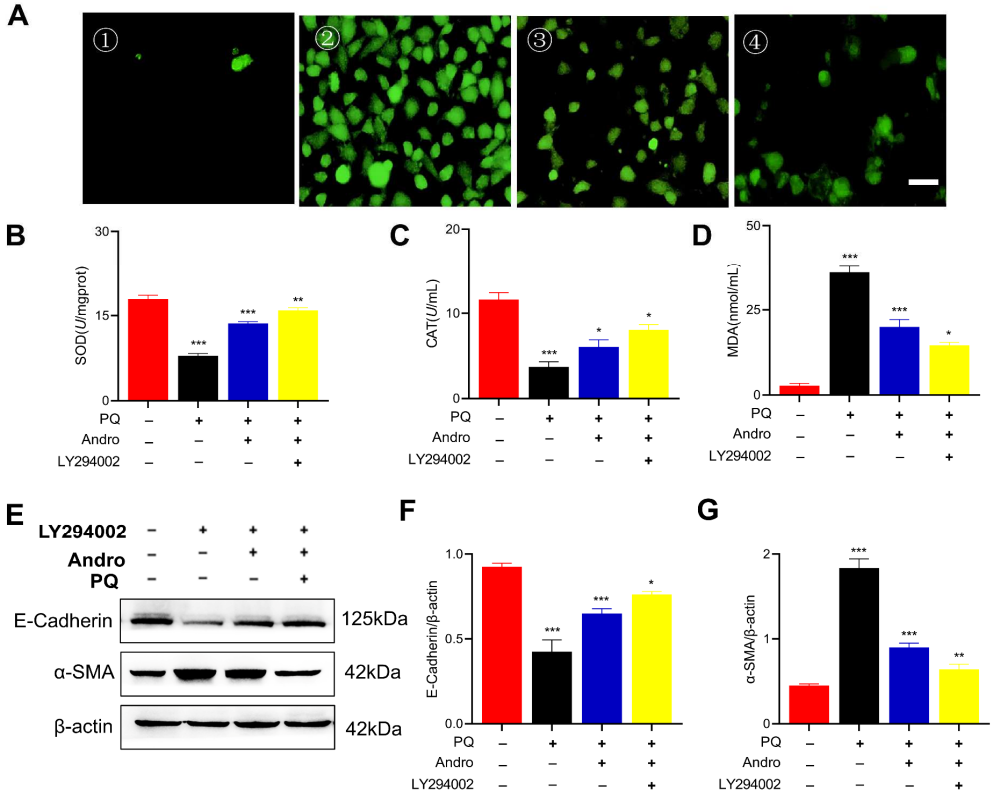

Fig. 5: Andro suppresses the PQ-induced oxidative stress and EMT in MLE-12 cells via the PI3K/Akt/PPARγ pathway. (A) ROS levels visualized by a fluorescent microscope (scale bar = 50 μm). (B-D) SOD, CAT, and MDA levels. (E) Western blot analysis of E-cadherin and α-SMA. (F) Quantitation of E-cadherin and (G) α-SMA expression. The statistics are presented as mean ± SD (N = 3). $^{*}P < 0.05$, $^{**}P < 0.01$.

This restricts the ability to fully evaluate the dose-response relationship, the optimal therapeutic window, and the long-term efficacy of Andro, particularly its potential antifibrotic effects. Second, mechanistic verification primarily relied on pharmacological inhibition, without genetic manipulation such as siRNA-mediated knockdown or gene overexpression. Therefore, the causal role of the PI3K/Akt and PPARγ pathways in mediating Andro's protective effects requires further validation through genetic approaches. Third, the study was limited to a murine model and a single epithelial cell line (MLE-12), which, although informative, may not fully recapitulate the complex pathophysiology of human PQ poisoning. Future studies should systematically assess different Andro doses and treatment time windows to better define its therapeutic range. Moreover, genetic strategies will be employed to elucidate downstream effectors of the PI3K/Akt axis and PPARγ, further clarifying the interplay between oxidative stress and EMT.

CONCLUSION

In conclusion, our study demonstrates that Andro significantly mitigates PQ-induced lung damage by simultaneously suppressing oxidative stress and EMT. Mechanistically, andro exerts its protective effects through suppression of the PI3K/Akt/PPARγ pathway, which serves as a central hub coordinating these two pathological processes. By elucidating this dual regulatory mechanism, our findings provide novel insights into PQ-induced lung toxicity and highlight Andro as a promising candidate for future therapeutic development. Importantly, additional studies are required to assess optimal dosing, long-term efficacy, safety, and translational relevance before any clinical application can be considered.

Acknowledgements
Not applicable

Authors' contributions
Degang Zhang and Jiayi Xiao performed the experiments, participated in data collection, and drafted the manuscript. Degang Zhang, Jiayi Xiao, Qinyi Cai, and Bo Zhao conducted statistical analysis, and contributed to the study design. Degang Zhang and Shengming Zhao contributed to data collection, analysis and interpretation and revised the manuscript. All authors critically reviewed and approved the final version of the manuscript.

Funding
The work was funded by the Natural Science Foundation of Gansu Province [grant number 25JRRA588]; the Gansu Province Administration of Traditional Chinese Medicine Project [grant number GZKP-2021-31]; the Gansu Health Industry Scientific Research Program [grant number GSWSKY2021-061]; Lanzhou University's Undergraduate Innovation and Entrepreneurship Project [grant numbers 20210050067 and 220210904030]; and Lanzhou University Second Hospital's Cuiying Scientific Training Program for Undergraduates [grant numbers CYXZ2022-35 and CYXZ2023-23].

Data availability statement
The datasets generated during and/or analysed during the current study are available from the corresponding author on reasonable request.

Ethical approval
This study was conducted with the approval of the Ethics Committee of Lanzhou University Second Hospital (Permit No. D2023-393) and conducted in accordance with the Ethical Principles in Animal Research. All procedures were performed following the applicable institutional and national guidelines and regulations.

Conflict of interest
The authors declare that they have no conflicts of interest related to this work.

REFERENCES

Abu-Eid R and Ward FJ (2021). Targeting the PI3K/Akt/mTOR pathway: A therapeutic strategy in COVID-19 patients. *Immunol. Lett.*, **240**: 1-8.

Amin F, Memarzia A, Roohbakhsh A, Shakeri F and Boskabady MH (2021). *Zataria multiflora* and pioglitazone affect systemic inflammation and oxidative stress induced by inhaled paraquat in rats. *Mediators Inflamm.*, **2021**: 5575059.

Andugulapati SB, Gourishetti K, Tirunavalli SK, Shaikh TB and Sistla R (2020). Biochanin-A ameliorates pulmonary fibrosis by suppressing the TGF-beta mediated EMT, myofibroblasts differentiation and collagen deposition in *in-vitro* and *in-vivo* systems. *Phytomedicine*, **78**: 153298.

Braga V (2016). Spatial integration of E-cadherin adhesion, signalling and the epithelial cytoskeleton. *Curr. Opin. Cell. Biol.*, **42**: 138-145.

Buckley NA, Fahim M, Raubenheimer J, Gawarammana IB, Eddleston M, Roberts MS and Dawson AH (2021). Case fatality of agricultural pesticides after self-poisoning in Sri Lanka: A prospective cohort study. *Lancet Glob. Health.*, **9**(6): e854-e862.

Burgos RA, Alarcon P, Quiroga J, Manosalva C and Hancke J (2020). Andrographolide, an anti-inflammatory multitarget drug: All roads lead to cellular metabolism. *Molecules*, **26**(1): 5.

Chen H, Chen N, Li F, Sun L, Du J, Chen Y, Cheng F, Li Y, Tian S, Jiang Q, Cui F and Tu Y (2020). Repeated radon exposure induced lung injury and epithelial-mesenchymal transition through the PI3K/AKT/mTOR pathway in human bronchial epithelial cells and mice. *Toxicol. Lett.*, **334**: 4-13.

Darby IA, Zakuan N, Billet F and Desmouliere A (2016).

The myofibroblast, a key cell in normal and pathological tissue repair. *Cell. Mol. Life. Sci.*, **73**(6): 1145-1157.

Gao F, Zhang Y, Yang Z, Wang M, Zhou Z, Zhang W, Ren Y, Han X, Wei M, Sun Z and Nie S (2020). Arctigenin suppressed epithelial-mesenchymal transition through Wnt3a/beta-catenin pathway in PQ-induced pulmonary fibrosis. *Front. Pharmacol.*, **11**: 584098.

Glaviano A, Foo ASC, Lam HY, Yap KCH, Jacot W, Jones RH, Eng H, Nair MG, Makvandi P, Geoerger B, Kulke MH, Baird RD, Prabhu JS, Carbone D, Pecoraro C, Teh DBL, Sethi G, Cavalieri V, Lin KH, Javidi-Sharifi NR, Toska E, Davids MS, Brown JR, Diana P, Stebbing J, Fruman DA and Kumar AP (2023). PI3K/AKT/mTOR signaling transduction pathway and targeted therapies in cancer. *Mol. Cancer.*, **22**(1): 138.

Jia R, Li T and Wang N (2021). Long noncoding RNA HOTAIR functions as ceRNA to regulate MMP2 in paraquat induced lung epithelial-mesenchymal transition. *Toxicology*, **461**: 152891.

Kanazawa LKS, Radulski DR, Pereira GS, Prickaerts J, Schwarting RKW, Acco A and Andreatini R (2021). Andrographolide blocks 50-kHz ultrasonic vocalizations, hyperlocomotion and oxidative stress in an animal model of mania. *J. Psychiatr. Res.*, **139**: 91-98.

Karkale S, Khurana A, Saifi MA, Godugu C and Talla V (2018). Andrographolide ameliorates silica induced pulmonary fibrosis. *Int. Immunopharmacol.*, **62**: 191-202.

Kumar G, Singh D, Tali JA, Dheer D and Shankar R (2020). Andrographolide: Chemical modification and its effect on biological activities. *Bioorg. Chem.*, **95**: 103511.

Lee HW, Jose CC and Cuddapah S (2021). Epithelial-mesenchymal transition: Insights into nickel-induced lung diseases. *Semin. Cancer. Biol.*, **76**: 99-109.

Lekei E, Ngowi AV, Kapeleka J and London L (2020). Acute pesticide poisoning amongst adolescent girls and women in northern Tanzania. *BMC Public Health.*, 20(1): 303.

Li J, Liu J, Yue W, Xu K, Cai W, Cui F, Li Z, Wang W and He J (2020). Andrographolide attenuates epithelial-mesenchymal transition induced by TGF-beta1 in alveolar epithelial cells. *J. Cell. Mol. Med.*, **24**(18): 10501-10511.

Lihua L, Yuning W, Henghui H, Xiang L, Min J, Zehao L, Lianjie L and Qian L (2023). Retrospective analysis of 217 fatal intoxication autopsy cases from 2009 to 2021: Temporal trends in fatal intoxication at Tongji center for medicolegal expertise, Hubei, China. *Front Public Health.*, **11**: 1137649.

Marconi GD, Fonticoli L, Rajan TS, Pierdomenico SD, Trubiani O, Pizzicannella J and Diomede F (2021). Epithelial-mesenchymal transition (EMT): The type-2 EMT in wound healing, tissue regeneration and organ fibrosis. *Cells*, **10**(7): 1587.

Memarzia A, Ghasemi SZ, Amin F, Gholamnezhad Z and Boskabady MH (2024). Effects of *Crocus sativus* and its constituent, safranal and pioglitazone, on systemic inflammation and oxidative stress induced by paraquat aerosol in rats. *Iran. J. Basic. Med. Sci.*, **27**(5): 640-646.

Memarzia A, Ghasemi SZ, Behrouz S and Boskabady MH (2023). The effects of *Crocus sativus* extract on inhaled paraquat-induced lung inflammation, oxidative stress, pathological changes and tracheal responsiveness in rats. *Toxicon*, **235**: 107316.

Meng X, Liu K, Xie H, Zhu Y, Jin W, Lu J and Wang R (2021). Endoplasmic reticulum stress promotes epithelial-mesenchymal transition via the PERK signaling pathway in paraquat-induced pulmonary fibrosis. *Mol. Med. Rep.*, **24**(1): 525.

Mussard E, Jousselin S, Cesaro A, Legrain B, Lespessailles E, Esteve E, Berteina-Raboin S and Toumi H (2020). *Andrographis paniculata* and its bioactive diterpenoids against inflammation and oxidative stress in keratinocytes. *Antioxidants (Basel)*, **9**(6): 530.

Qin L, Huang J, Feng Y, Zhao B, Guo L and Xie J (2024). Spatiotemporal visualization of paraquat distribution, troxicokinetics and its detoxification in zebrafish using matrix-assisted laser desorption ionization mass spectrometry imaging. *Chem. Res. Toxicol.*, **37**(2): 385-394.

Somu B, Halkur Shankar S, Baitha U and Biswas A (2020). Paraquat poisoning. *QJM*, **113**(10): 752.

Spagnolo P, Kropski JA, Jones MG, Lee JS, Rossi G, Karampitsakos T, Maher TM, Tzouvelekis A and Ryerson CJ (2021). Idiopathic pulmonary fibrosis: Disease mechanisms and drug development. *Pharmacol. Ther.*, **222**: 107798.

Tyagi N, Singh D. K, Dash D and Singh R (2019). Curcumin modulates paraquat-induced epithelial to mesenchymal transition by regulating transforming growth factor-beta (TGF-beta) in A549 Cells. *Inflammation*, **42**(4): 1441-1455.

Wu N, Li Z, Wang J, Geng L, Yue Y, Deng Z, Wang Q and Zhang Q (2021). Low molecular weight fucoidan attenuating pulmonary fibrosis by relieving inflammatory reaction and progression of epithelial-mesenchymal transition. *Carbohydr. Polym.*, **273**: 118567.

Xia J, Xiong Z, Guo J, Wang Y, Luo Y, Sun Y, Guo Z, Lu B, Zhang T and Sun W (2022). Study of paraquat-induced pulmonary fibrosis using biomimetic micro-lung chips. *Biofabrication*, **15**(1): doi: 10.1088/1758-5090/ac999e.

Yi JH, Zhang ZC, Zhang MB, He X, Lin HR, Huang HW, Dai HB and Huang YW (2021). Role of epithelial-to-mesenchymal transition in the pulmonary fibrosis induced by paraquat in rats. *World. J. Emerg. Med.*, **12**(3): 214-220.

Yoshida T, Uchiyama A, Matsuura N, Mashimo T and Fujino Y (2012). Spontaneous breathing during lung-protective ventilation in an experimental acute lung injury model: High transpulmonary pressure associated

with strong spontaneous breathing effort may worsen lung injury. *Crit. Care. Med.*, **40**(5): 1578-1585.

Zhang D, Shen F, Ma S, Nan S, Ma Y, Ren L, Li H and Yu Q (2023). Andrographolide alleviates paraquat-induced acute lung injury by activating the Nrf2/HO-1 pathway. *Iran. J. Basic. Med. Sci.*, **26**(6): 653-661.